ACS APPLIED MATERIALS & INTERFACES

RESEARCH ARTICLE

www.acsami.org

Heterostructured Bismuth Molybdate Composite: Preparation and Improved Photocatalytic Activity under Visible-Light Irradiation

Jia Ren, Wenzhong Wang,* Meng Shang, Songmei Sun, and Erping Gao

State Key Laboratory of High Performance Ceramics and Superfine Microstructure, Shanghai Institute of Ceramics, Chinese Academy of Sciences, 1295 Dingxi Road, Shanghai 200050, People's Republic of China

Supporting Information

ABSTRACT: A heterostructured photocatalyst containing the same Bi, Mo, and O elements ($Bi_{3.64}Mo_{0.36}O_{6.55}/Bi_2MoO_6$) was realized by a facile hydrothermal method. The heterostructured composite was characterized by powder X-ray diffraction, selected-area electron diffraction, scanning electron microscopy, and high-resolution electron microscopy. The $Bi_{3.64}Mo_{0.36}O_{6.55}/Bi_2MoO_6$ composite exhibited notable enhanced photocatalytic activity compared to Bi_2MoO_6 or $Bi_{3.64}Mo_{0.36}O_{6.55}$ in the photocatalytic degradation of rhodamine B and phenol under visible-light irradiation. More interestingly, it is found that the heterostructured composite could mineralize organic substances into CO_2 efficiently. This study offered a clue for the design of an efficient photocatalyst in the application of environmental treatment.

KEYWORDS: heterostructure, bismuth molybdate composite, photocatalytic activity

INTRODUCTION

Photocatalysis over semiconductors using solar energy has attracted extensive attention in the splitting of water and the degradation of organic pollutants.[1−3] However, how to improve the photocatalytic efficiency to meet practical requirements is still a big challenge for solving the global energy and environmental issues. Recently, semiconductor-based heterostructures have received a great deal of attention, arising from the following two considerations.[4,5] First, control over the composition of wide-band-gap energy semiconductors can realize the effective utilization of solar energy. Metal−oxide semiconductors such as TiO_2 and ZnO coupling with a narrow-band-gap semiconductor have been studied intensively to extend the photoresponding range.[6−9] Second, charge transfer from one semiconductor to another can lead to efficient charge separation by reducing the electron−hole pair recombination.[10,11]

Generally, heterostructured composites, which contain two or more different photocatalysts such as Cu_2O/TiO_2, WO_3/TiO_2, CdS/TiO_2, $Co_2O_3/BiVO_4$, or $AgBr/Ag/Bi_2WO_6$, were studied extensively, and they exhibited enhanced photocatalytic activities.[12−16] However, a heterostructured photocatalyst containing the same elements is rarely investigated. For the composite photocatalysts, the interface should be very important, which is the key pass connecting different components. Many methods have been carried out to obtain composites, i.e., the electrochemical method, electrospinning, physical or chemical vapor deposition, etc.[12,13,17,18] In addition, most of the combination processes were realized through two or more steps. Hydrothermal synthesis not only is a mild and facile process but also offers a high degree of crystallinity and controllable particle size of the products.

γ-Bi_2MoO_6, as an Aurivillius-phase perovskite represented by $(Bi_2O_2)^{2+}(A_{n-1}B_nO_{3n+1})^{2-}$ (A = Ba, Bi, Pb, etc.; B = Ti, Nb, W, Mo, etc.), possesses unique layered structures in which perovskite slabs of $(A_{n-1}B_nO_{3n+1})^{2-}$ are sandwiched between $(Bi_2O_2)^{2+}$ layers. Its dielectric, ion-conductive, and catalytic properties have attracted attention.[19−21] Also, its visible-light-responsive property makes Bi_2MoO_6 worthy of consideration as an advanced material for photocatalytic application. Many studies about the effects of the crystallinity, size, and morphology on the photocatalytic property of Bi_2MoO_6 synthesized by the hydrothermal process have been carried out.[22−24] $Bi_{3.64}Mo_{0.36}O_{6.55}$ with a cubic phase is another kind of bismuth molybdate. There are a few investigations concerning $Bi_{3.64}Mo_{0.36}O_{6.55}$ as a photocatalyst. Synthetic processes, such as low-temperature molten salt and microwave-assisted methods, have been studied for the preparation for $Bi_{3.64}Mo_{0.36}O_{6.55}$.[25,26] In this study, a heterostructured photocatalyst, $Bi_{3.64}Mo_{0.36}O_{6.55}/Bi_2MoO_6$, with the same Bi, Mo, and O elements was realized by a simple hydrothermal method and characterized in detail. The photocatalytic activity of a $Bi_{3.64}Mo_{0.36}O_{6.55}/Bi_2MoO_6$ composite was investigated in comparison with that of pure Bi_2MoO_6 and $Bi_{3.64}Mo_{0.36}O_{6.55}$ obtained by the hydrothermal method through the photocatalytic degradation of respectively an organic dye of rhodamine B (RhB) and a colorless model pollutant of phenol under visible-light irradiation. The results revealed that the $Bi_{3.64}Mo_{0.36}O_{6.55}/Bi_2MoO_6$ composite exhibits the best photocatalytic performance in the degradation of both RhB and phenol. To the best of our knowledge, investigations on the photocatalytic activity of a bismuth molybdate heterostructured composite have not been attempted yet.

EXPERIMENTAL SECTION

All of the reagents were of analytical grade and were used without any further purification. In a typical procedure, 0.970 g of $Bi(NO_3)_3 \cdot 5H_2O$ was first dissolved in 5 mL of a 4 M nitric acid solution and then diluted

Received: April 1, 2011
Accepted: June 15, 2011
Published: June 15, 2011

to 18 mL with deionized water. A total of 0.242 g of $Na_2MoO_4 \cdot 2H_2O$ was dissolved in 18 mL of deionized water. A white precipitate was formed when the Na_2MoO_4 solution was added dropwise to the above mixed solution. The pH value of the precursor suspension was changed from 5 to 11 by the addition of a 2 M NaOH solution when necessary. The samples denoted as p5, p6, p6.6, p7, p9, and p11 represent the samples prepared at pH values of 5, 6, 6.6, 7, 9, and 11, respectively. After being stirred for 3 h, the suspension was transferred to a 50 mL Teflon-lined autoclave up to 80% of the total volume. Then the autoclave was sealed in a stainless steel tank and kept under a series of experiment conditions. Subsequently, the autoclave was cooled to room temperature naturally. The temperature series of samples denoted as T140, T160, and T180 represent the samples prepared at 140, 160, and 180 °C for 12 h with a pH value of 7. The resulting samples were collected, washed with deionized water, and dried at 60 °C in air. All of the time series of samples were prepared at 160 °C with a pH value of 7 for different hours.

The powder X-ray diffraction (XRD) patterns of the as-synthesized samples were recorded on a D/MAX 2250 V diffractometer (Rigaku, Japan) using monochromatized Cu Kα (λ = 0.154 18 nm) radiation under 40 kV and 100 mA and with 2θ ranging from 10° to 70°. UV−vis diffuse-reflectance spectra of the samples were obtained on an UV−vis spectrophotometer (Hitachi U-3010) using $BaSO_4$ as the reference. The morphologies and microstructures of as-prepared samples were analyzed by a field-emission scanning electron microscope (JEOL JSM-6700F). Transmission electron microscopy (TEM) and high-resolution transmission electron microscopy (HRTEM) images were obtained using a JEOL JEM-2100F field-emission electron microscope at an acceleration voltage of 200 kV. Nitrogen adsorption−desorption measurements were conducted at 77.35 K on a Micromeritics Tristar 3000 analyzer after the samples were degassed at 150 °C for 3 h. The Brunauer−Emmett−Teller (BET) surface areas of the products were estimated using the adsorption data.

Photocurrent measurements were carried out on an Electrochemical Station CHI660D in a standard three-electrode system. A total of 25 mg of the photocatalyst was suspended in distilled water (50 mL) containing acetate (0.1 M) and Fe^{3+} (0.1 mM) as an electron donor and acceptor, respectively. A platinum plate (both sides exposed to the solution), a saturated calomel electrode (SCE), and a platinum wire were immersed in the reactor as working (collector), reference, and counter electrodes, respectively. Photocurrents were measured by applying a potential (+1 V vs SCE) to the platinum electrode using a potentiostat (EG&G).

The photocatalytic activities of the samples were evaluated by the degradation of RhB and phenol under visible-light irradiation of a 500 W xenon lamp with a 420 nm cutoff filter. The experiments were carried out at room temperature. A total of 0.05 g of the as-prepared sample was added to 10 mg/L of RhB with a magnetic stirrer to prevent settling of the photocatalysts. Before illumination, the solution was stirred in the dark overnight in order to reach the adsorption−desorption equilibrium of RhB on the photocatalysts. The concentrations of RhB were monitored with a Hitachi UV-3010PC UV−vis spectrophotometer in terms of the absorbance at 553 nm during the photodegradation process. For the degradation of phenol, 0.05 g of the photocatalyst was added to 100 mL of a phenol solution (7 mg/L). The reaction was carried out in a gas-closed reactor at room temperature (capacity 600 mL). The absorption spectrum of the centrifugated solution was recorded using a Hitachi U-3010 UV−vis spectrophotometer. The concentration of carbon dioxide was determined by using a gas chromatograph equipped with a flame ionization detector (N_2 carrier) and a catalytic conversion furnace.

RESULTS AND DISCUSSION

The formation of bismuth molybdate was well confirmed by XRD analysis. As shown in Figure 1, all of the diffraction peaks of

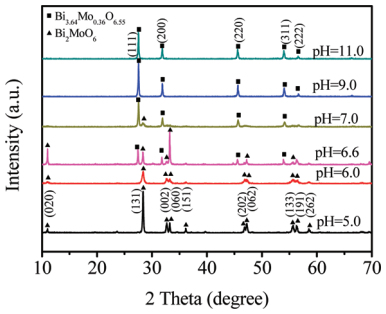

Figure 1. XRD patterns of the samples prepared at 160 °C for 12 h at different pH values.

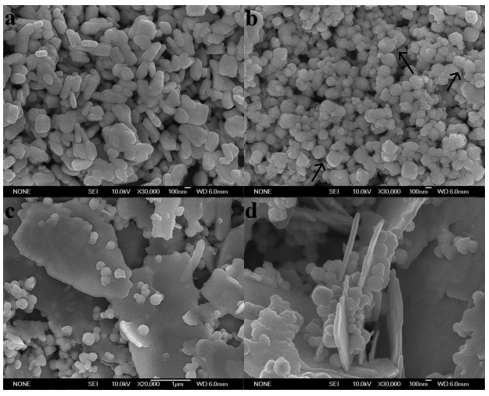

Figure 2. Typical SEM images of three kinds of bismuth molybdate samples prepared at 160 °C for 12 h: (a) Bi_2MoO_6 (pH = 5); (b) $Bi_{3.64}Mo_{0.36}O_{6.55}$ (pH = 9); (c and d) $Bi_{3.64}Mo_{0.36}O_{6.55}/Bi_2MoO_6$ composite (pH = 6.6).

the XRD patterns were indexed as orthorhombic Bi_2MoO_6 and cubic $Bi_{3.64}Mo_{0.36}O_{6.55}$. After refinement, the cell parameters of Bi_2MoO_6 were calculated as a = 5.503 Å, b = 16.207 Å, and c = 5.484 Å, which correspond to the standard pattern (JCPDS 21-0102 with a = 5.502 Å, b = 16.213 Å, and c = 5.483 Å). Also, the cell parameters of $Bi_{3.64}Mo_{0.36}O_{6.55}$ are $a = b = c$ = 5.639 Å after refinement, which are in agreement with the standard pattern (JCPDS 43-0446 with a = 5.639 Å). No other peaks from possible impurities are detected.

Bismuth molybdates were characterized by scanning electron microscopy (SEM). Figure 2a shows that the as-prepared Bi_2MoO_6 consists of platelet-type particles with a length of up to 400 nm. Octahedron-like nanoparticles are observed in the image of $Bi_{3.64}Mo_{0.36}O_{6.55}$, implying its cubic structure (Figure 2b). It can be clearly seen from Figure 2c,d that the $Bi_{3.64}Mo_{0.36}O_{6.55}/Bi_2MoO_6$ composite is composed of sheets with the size of 2 μm and nanoparticles with the size of 100 nm embedded in the sheets. To further confirm the composition of the composite, the sample was characterized by TEM and selected-area electron diffraction (SAED) analysis. As shown in Figure 3a, the sample exhibits two different kinds of morphologies. The SAED pattern (Figure 3b) taken along the [011] direction on the area marked 1 in Figure 3a indicated that the sheet is a single crystal. The angle between the (0−11) and (100) planes was 90.0°, which is consistent with the crystal structure of Bi_2MoO_6. The SAED pattern (Figure 3c) was taken along the [110] direction on the area marked 2 in Figure 3a, indicating that the nanoparticle is a single crystal. Also, the angle between the (1−11) and (1−1−1)

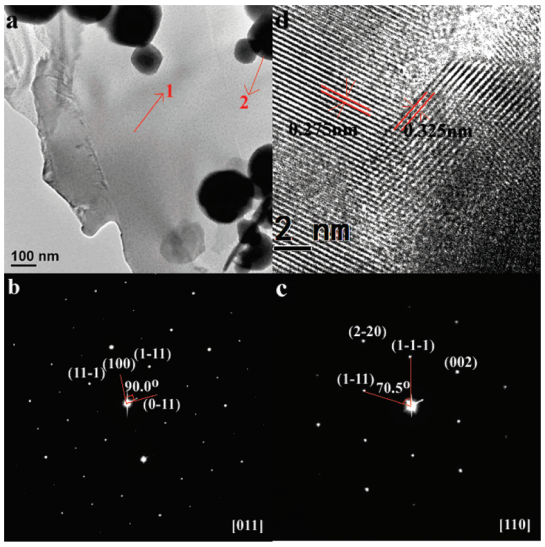

Figure 3. (a) TEM image of a sample $Bi_2MoO_6/Bi_{3.64}Mo_{0.36}O_{6.55}$ composite with a pH value of 6.6, (b) SAED pattern taken on the area marked 1 in part a, (c) SAED pattern taken on the area marked 2 in part a, (d) HRTEM image of a $Bi_2MoO_6/Bi_{3.64}Mo_{0.36}O_{6.55}$ composite.

planes was 70.5°, which is consistent with the crystal structure of $Bi_{3.64}Mo_{0.36}O_{6.55}$. As shown in the HRTEM image, the lattice fringes with interplanar spacing of 0.275 nm corresponded to the (200) plane of Bi_2MoO_6, while the fringes of $d = 0.325$ nm matched the (1−11) crystallographic planes of cubic $Bi_{3.64}Mo_{0.36}O_{6.55}$ particles. On the basis of the above analysis, it can be confirmed that a $Bi_{3.64}Mo_{0.36}O_{6.55}/Bi_2MoO_6$ composite with heterostructure was obtained in our synthetic process.

The pH value is the key factor in the formation of bismuth molybdate. The samples prepared at pH values ranging from 5 to 11 are assigned to three compositions, namely, pure Bi_2MoO_6, pure $Bi_{3.64}Mo_{0.36}O_{6.55}$, and the $Bi_{3.64}Mo_{0.36}O_{6.55}/Bi_2MoO_6$ composite. It is clear that the samples p5 and p6 are pure Bi_2MoO_6. When the pH value was increased to 6.6 and 7, the XRD pattern showed mixed phases of Bi_2MoO_6 and $Bi_{3.64}Mo_{0.36}O_{6.55}$. As the pH value was further increased to 9, the XRD pattern exhibited a pure $Bi_{3.64}Mo_{0.36}O_{6.55}$ phase, without any detectable Bi_2MoO_6, and so did sample p11. On the basis of these results, we can conclude that the acidic condition is favorable for the formation of Bi_2MoO_6, while the alkaline medium favors the formation of $Bi_{3.64}Mo_{0.36}O_{6.55}$. The $Bi_{3.64}Mo_{0.36}O_{6.55}/Bi_2MoO_6$ composite can only be obtained when the pH value is appropriate. The effects of the temperature and time of hydrothermal treatment on the synthesis of the composite photocatalyst were also investigated. With a pH value of 7.0, the sample prepared at 140, 160, and 180 °C was the $Bi_{3.64}Mo_{0.36}O_{6.55}/Bi_2MoO_6$ composite (Figure S1 in the Supporting Information). However, the ratios of the two phases were different, which was reflected by the different relative intensities of the diffraction peak of the two phases. In comparison with the effect brought by the pH value, the differences arising from the time of hydrothermal treatment are negligible (Figure S2 in the Supporting Information).

Diffuse-reflectance spectroscopy (DRS) is an important method for characterizing the electronic states and optical properties of semiconductor materials. The DRS spectra of as-prepared bismuth molybdates are shown in Figure 4. The samples exhibited an intense absorption in the visible-light range, which suggests the

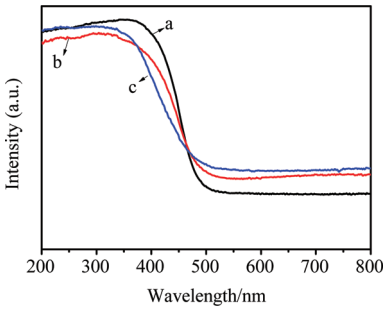

Figure 4. UV−vis absorption spectra of the bismuth molybdate samples prepared at 160 °C for 12 h: (a) Bi_2MoO_6 (pH = 5); (b) $Bi_{3.64}Mo_{0.36}O_{6.55}/Bi_2MoO_6$ composite (pH = 7); (c) $Bi_{3.64}Mo_{0.36}O_{6.55}$ (pH = 9).

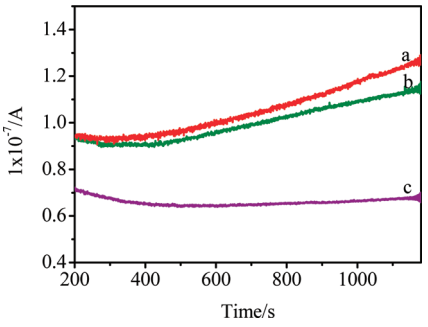

Figure 5. Photocurrent generation under visible light in aqueous photocatalyst suspensions with acetate and Fe^{3+} as an electron donor and an acceptor, respectively: (a) $Bi_{3.64}Mo_{0.36}O_{6.55}/Bi_2MoO_6$ composite (160 °C for 12 h, pH = 7); (b) Bi_2MoO_6 (160 °C for 12 h, pH = 5); (c) $Bi_{3.64}Mo_{0.36}O_{6.55}$ (160 °C for 12 h, pH = 9).

property of being photoactive under visible-light irradiation. The steep shape of the spectra suggests that the light absorption is due to a band-gap transition instead of a transition induced by impurity levels.[27] The absorption edges of Bi_2MoO_6, a $Bi_{3.64}Mo_{0.36}O_{6.55}/Bi_2MoO_6$ composite, and $Bi_{3.64}Mo_{0.36}O_{6.55}$ are located around 510, 538, and 547 nm, respectively. Their band gaps are estimated to be 2.43, 2.30, and 2.26 eV from the onset of absorption edges. The band gap was mainly influenced by the coordination number of the oxygen ions to a molybdenum ion. The as-prepared Bi_2MoO_6 in this study exhibited a narrower band gap compared with that reported by Kudo and co-workers. Visible-light adsorption of γ-Bi_2MoO_6 was revealed by the plane-wave-based DFT method to be due to a transition from the valence band consisting of the O 2p orbitals to the conduction band derived from the primary Mo 4d orbitals in MoO_6 octahedra and the secondary Bi 6p orbitals.[28]

To demonstrate that the heterostructured composite semiconductors were preferred for efficient charge separation, the photocurrents generated on the samples with different phases were measured. Generally, the value of the photocurrent indirectly reflects the semiconductor's ability to generate and transfer a photogenerated charge carrier under irradiation, which correlates with the photocatalytic activity.[29] It is shown in Figure 5 that the Bi_2MoO_6 and $Bi_{3.64}Mo_{0.36}O_{6.55}/Bi_2MoO_6$ spectra are more efficient in photocurrent generation compared to $Bi_{3.64}Mo_{0.36}O_{6.55}$, and the composite $Bi_{3.64}Mo_{0.36}O_{6.55}/Bi_2MoO_6$ generates higher photocurrent than Bi_2MoO_6. Therefore, the composite composition

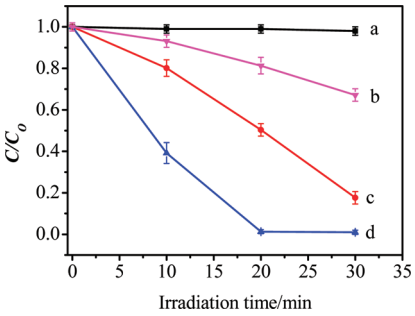

Figure 6. Plot of the photodegradation of RhB as a function of the irradiation time for the blank and the samples prepared at 160 °C for 12 h: (a) RhB photolysis; (b) $Bi_{3.64}Mo_{0.36}O_{6.55}$ (pH = 9); (c) Bi_2MoO_6 (pH = 5); (d) $Bi_2MoO_6/Bi_{3.64}Mo_{0.36}O_{6.55}$ composite (pH = 7.0).

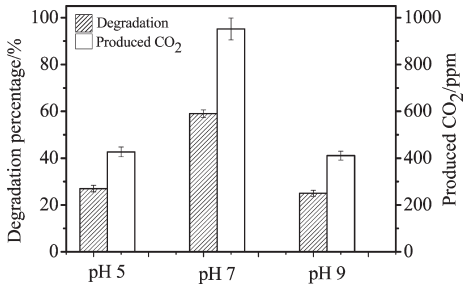

Figure 7. Photodegradation of phenol on samples p5 (Bi_2MoO_6), p7 ($Bi_{3.64}Mo_{0.36}O_{6.55}/Bi_2MoO_6$), and p9 ($Bi_{3.64}Mo_{0.36}O_{6.55}$) after 6 h of visible-light irradiation.

enhanced the charge carrier transfer and reduced the electron−hole recombination. It is assumed that interactions between $Bi_{3.64}Mo_{0.36}O_{6.55}$ and Bi_2MoO_6 are favorable for enhancing the photocatalytic activity of $Bi_{3.64}Mo_{0.36}O_{6.55}/Bi_2MoO_6$.

The photocatalytic activity of the composite photocatalyst $Bi_{3.64}Mo_{0.36}O_{6.55}/Bi_2MoO_6$ was compared with those of Bi_2MoO_6 and $Bi_{3.64}Mo_{0.36}O_{6.55}$ by photocatalytic dye degradation under visible-light irradiation ($\lambda > 420$ nm). RhB was chosen as a representative model pollutant. The establishment of adsorption−desorption equilibrium was obtained under continuous stirring overnight before the degradation reaction was carried out. The absorption of an aqueous solution of RhB at a wavelength of 553 nm decreased under visible-light irradiation, which suggested an apparent decrease of RhB. Figure 6 displays a plot of the photodegradation extent of RhB molecules (monitored at 553 nm) as a function of the irradiation time by different bismuth molybdate samples. C is the absorption of RhB at a wavelength of 553 nm during the photocatalytic process, and C_0 is the absorption after adsorption equilibrium on photocatalysts. The photolysis of RhB is quite slow under xenon lamp irradiation without photocatalysts. The $Bi_{3.64}Mo_{0.36}O_{6.55}/Bi_2MoO_6$ composite exhibits the highest photocatalytic activity. Up to 99% of RhB was degraded under visible-light irradiation after 30 min in the presence of the $Bi_{3.64}Mo_{0.36}O_{6.55}/Bi_2MoO_6$ composite, while the photocatalytic degradation rates are 82% and 33% for the photocatalysts Bi_2MoO_6 and $Bi_{3.64}Mo_{0.36}O_{6.55}$ with otherwise identical conditions, respectively.

In addition, it is found that the $Bi_{3.64}Mo_{0.36}O_{6.55}/Bi_2MoO_6$ composite in different ratios of Bi_2MoO_6 to $Bi_{3.64}Mo_{0.36}O_{6.55}$ also exhibits different photocatalytic activities (Figure S3 in the Supporting Information). Totals of 98%, 61%, and 81% of RhB are degraded in 10 min on the samples T140, T160, and T180, respectively. It is obvious that the sample T140 with the largest ratio of Bi_2MoO_6 to $Bi_{3.64}Mo_{0.36}O_{6.55}$ shows the highest photocatalytic activity in degrading RhB, while the sample T160 with the smallest ratio in which $Bi_{3.64}Mo_{0.36}O_{6.55}$ is the major phase exhibits the lowest photocatalytic activity. On the basis of the above analysis, we conclude that the $Bi_{3.64}Mo_{0.36}O_{6.55}/Bi_2MoO_6$ composite possesses higher photocatalytic activity compared with the pure Bi_2MoO_6 and $Bi_{3.64}Mo_{0.36}O_{6.55}$. Also, the ratio of Bi_2MoO_6 to $Bi_{3.64}Mo_{0.36}O_{6.55}$ affects the photocatalytic activity of the composite.

Considering that photosensitization exists when organic dyes such as RhB were used as model pollutants, which also absorb visible light and contribute to photodegradation, a colorless compound would be a better choice to reveal the photocatalytic activities of the products. Thus, besides RhB, phenol was also selected to evaluate the photocatalytic properties of the bismuth molybdate composites so as to exclude the influence of photosensitization. To confirm that phenol is really mineralized by photocatalysis, the concentration of produced CO_2 was detected, which reflects the extent of mineralization of phenol in the photocatalytic degradation process. As shown in Figure 7, the photocatalytic activities of Bi_2MoO_6 and $Bi_{3.64}Mo_{0.36}O_{6.55}$ were low in degrading phenol under visible-light irradiation. By contrast, the $Bi_{3.64}Mo_{0.36}O_{6.55}/Bi_2MoO_6$ composite exhibited an obviously enhanced photocatalytic activity. A total of 59% of phenol was degraded, and about 952 ppm of CO_2 was produced after 6 h of irradiation. Up to 90% of the degraded phenol was mineralized into CO_2 during the photocatalytic process. The enhanced photocatalytic activity of the $Bi_{3.64}Mo_{0.36}O_{6.55}/Bi_2MoO_6$ heterostructured composite should be correlated with the synergetic effect between $Bi_{3.64}Mo_{0.36}O_{6.55}$ and Bi_2MoO_6. Moreover, the BET specific surface area of the $Bi_{3.64}Mo_{0.36}O_{6.55}/Bi_2MoO_6$ composite was measured to be ~10 m^2/g, while Bi_2MoO_6 and $Bi_{3.64}Mo_{0.36}O_{6.55}$ were 4 and 6 m^2/g, respectively. The higher photocatalytic activity of the $Bi_{3.64}Mo_{0.36}O_{6.55}/Bi_2MoO_6$ composite might be related to its higher BET surface area.

CONCLUSIONS

The heterostructured composite $Bi_{3.64}Mo_{0.36}O_{6.55}/Bi_2MoO_6$ was successfully synthesized by the hydrothermal method. By tuning of the pH value of the reaction system, the composition of the target compounds could be controlled. The hydrothermal temperature also affected the composition of bismuth molybdates. Photocatalysis investigations reveal that the $Bi_{3.64}Mo_{0.36}O_{6.55}/Bi_2MoO_6$ composite exhibits the highest photocatalytic activity compared with the pure Bi_2MoO_6 and pure $Bi_{3.64}Mo_{0.36}O_{6.55}$. The photocatalytic activity improvement could be attributed to the higher surface area and the enhancement of the carrier mobility in the heterostructured composite material. In addition, the photocatalytic activity of the $Bi_{3.64}Mo_{0.36}O_{6.55}/Bi_2MoO_6$ composite is related to the ratios of the two phases. The $Bi_{3.64}Mo_{0.36}O_{6.55}/Bi_2MoO_6$-based heterostructured materials are promising visible-light-driven catalysts.

ASSOCIATED CONTENT

Supporting Information. XRD patterns and a plot of the photodegradation of RhB as a function of the irradiation time. This material is available free of charge via the Internet at http://pubs.acs.org.

AUTHOR INFORMATION

Corresponding Author
*E-mail: wzwang@mail.sic.ac.cn. Fax: +86-21-5241-3122.

ACKNOWLEDGMENT

This work was supported by the National Natural Science Foundation of China (Grants 50972155 and 50902144), the National Basic Research Program of China (Grants 2007CB613305 and 2010CB933503), and the Nanotechnology Programs of Science and Technology Commission of Shanghai (Grant 0952 nm00400).

REFERENCES

(1) Ollis, D. F.; Hsiao, C. Y.; Budiman, L.; Lee, C. L. *J. Catal.* **1984**, *88*, 89–96.
(2) Legrini, O.; Oliveros, E.; Braun, A. M. *Chem. Rev.* **1993**, *93*, 671–698.
(3) Augugliaro, V.; Palmisano, L.; Schiavello, M.; Sclafani, A.; Marchese, L.; Martra, G.; Miano, F. *Appl. Catal.* **1991**, *69*, 323–340.
(4) Shang, M.; Wang, W. Z.; Yin, W. Z.; Ren, J.; Sun, S. M.; Zhang, L. *Chem.—Eur. J.* **2010**, *16*, 11412–11419.
(5) Kim, T. W.; Ha, H. W.; Paek, M. J.; Hyun, S. H.; Choy, J. H.; Hwang, S. J. *J. Mater. Chem.* **2010**, *20*, 3238–3245.
(6) Tak, Y.; Hong, S. J.; Lee, J. S.; Yong, K. *Cryst. Growth Des.* **2009**, *9*, 2627–2632.
(7) Tak, Y.; Kim, H.; Lee, D.; Yong, K. *Chem. Commun.* **2008**, 4585–4587.
(8) Kim, T. W.; Hur, S. G.; Hwang, S. J.; Park, H.; Choi, W.; Choy, J. H. *Adv. Funct. Mater.* **2007**, *17*, 307–314.
(9) Kamat, P. V. *Chem. Rev.* **1993**, *93*, 267–300.
(10) Gopidas, K. R.; Bohorquez, M.; Kamat, P. V. *J. Phys. Chem.* **1990**, *94*, 6435–6440.
(11) Evans, J. E.; Springer, K. W.; Zhang, J. Z. *J. Chem. Phys.* **1994**, *101*, 6222–6225.
(12) Long, M.; Cai, W. M.; Cai, J.; Zhou, B. X.; Chai, X. Y.; Wu, Y. H. *J. Phys. Chem. B* **2006**, *110*, 20211–20216.
(13) Zhang, Y. G.; Ma, L. L.; Li, J. L.; Yu, Y. *Environ. Sci. Technol.* **2007**, *41*, 6264–6269.
(14) Papp, J.; Soled, S.; Dwight, K.; Wold, A. *Chem. Mater.* **1994**, *6*, 496–500.
(15) Jang, J. S.; Li, W.; Oh, S. H.; Lee, J. S. *Chem. Phys. Lett.* **2006**, *425*, 278–282.
(16) Zhang, L. S.; Wong, K. H.; Chen, Z. G.; Yu, J. C.; Zhao, J. C.; Hu, C.; Chan, C. Y.; Wong, P. K. *Appl. Catal., A* **2009**, *363*, 221–229.
(17) Ostermann, R.; Li, D.; Yin, Y. D.; McCann, J. T.; Xia, Y. N. *Nano Lett.* **2006**, *6*, 1297–1302.
(18) Wang, H.; Quan, X.; Yu, H. T.; Chen, S. *Carbon* **2008**, *46*, 1126–1132.
(19) Hamada, M.; Tabata, H.; Kawai, T. *Thin Solid Films* **1997**, *306*, 6–9.
(20) Murugan, R. *Physica B* **2004**, *352*, 227–232.
(21) Galvan, D. H.; Fuentes, S.; Avalos-Borja, M.; Cota-Araiza, L.; Cruz-Reyes, J.; Early, E. A.; Maple, M. B. *Catal. Lett.* **1993**, *18*, 273–281.
(22) Xu, C.; Zou, D.; Wang, L.; Luo, H.; Ying, T. *Ceram. Int.* **2009**, *35*, 2099–2102.
(23) Gruar, R.; Tighe, C. J.; Reilly, L. M.; Sankar, G.; Darr, J. A. *Solid State Sci.* **2010**, *12*, 1683–1686.
(24) Zhang, L.; Xu, T.; Zhao, X.; Zhu, Y. *Appl. Catal., B: Environ.* **2010**, *98*, 138–146.
(25) Xie, L.; Liu, Z.; Zhang, J.; Ma, J. *J. Alloys Compd.* **2010**, *503*, 159–162.
(26) Duan, F.; Zheng, Y.; Chen, M. Q. *Mater. Lett.* **2010**, *65*, 191–193.
(27) Kudo, A.; Tsuji, I.; Kato, H. *Chem. Commun.* **2002**, 1958–1959.
(28) Shimodaira, Y.; Kato, H.; Kobayashi, H.; Kudo, A. *J. Phys. Chem. B* **2006**, *110*, 17790–17797.
(29) Kim, H. G.; Borse, P. H.; Choi, W. Y.; Lee, J. S. *Angew. Chem., Int. Ed.* **2005**, *44*, 4585–4589.